

Cite this: *Chem. Sci.*, 2025, 16, 2751

All publication charges for this article have been paid for by the Royal Society of Chemistry

Mechanistic insights into the visible-light-driven O-arylation of carboxylic acids catalyzed by xanthine-based nickel complexes†

Rafael E. Rodriguez-Lugo,[‡]*^a Joan Sander,[§]*^{ab} Simon Dietzmann,^a Thomas Rittner,[‡]*^c Jannes Rückel,^a Vanessa R. Landaeta,[‡]*^a Jiyong Park,[‡]*^{bd} Patrick Nuernberger,[‡]*^c Mu-Hyun Baik[‡]*^{bd} and Robert Wolf[‡]*^a

We present a photocatalytic protocol for the O-arylation of carboxylic acids using nickel complexes bearing C8-pyridyl xanthenes. Our studies suggest that the underlying mechanism operates independently of external photosensitizers. Stoichiometric experiments and crystallographic studies characterize the catalytically relevant Ni complexes. Spectroscopic and computational investigations propose a thermally controlled Ni(II)/Ni(III) cycle followed by a photochemical regeneration of Ni(II) species. Furthermore, the pathways leading to the hydrodehalogenation of aryl halides, the comproportionation of Ni(II) and Ni(III) species, the dimerization of Ni(II) intermediates and the influence of the counter ion on the cross-coupling reaction are unveiled. These investigations offer a comprehensive mechanistic understanding of the photocatalytic cross-coupling reaction catalyzed by a single Ni species and highlight key aspects of nickel-catalyzed metallaphotoredox reactions.

Received 27th June 2024

Accepted 25th December 2024

DOI: 10.1039/d4sc04257c

rsc.li/chemical-science

Introduction

Metallaphotoredox catalysis effectively merges photoredox catalysis and transition metal catalysis, enabling challenging bond formations and novel chemical reactions under benign conditions.^{1,2} While a variety of transition metals have been employed, nickel catalysis has enjoyed particular success in facilitating the formation of new C–O, C–N, C–S, and C–C bonds through photoactivated cross-coupling reactions.^{1,3–11} These dual photocatalytic strategies often use commercially available bipyridine chelates combined with external photosensitizers.¹²

Among these motifs, 4,4'-di-*tert*-butyl-2,2'-bipyridine (dtbbpy) usually is the ligand of choice.^{13–15} In addition, engineered photoactive bipyridine-like scaffolds have also proven effective.¹⁶

Aryl-esterification is a versatile C–O coupling reaction with wide-ranging applications in fine chemical, pharmaceutical, and natural product synthesis.^{17–20} Numerous approaches have been investigated for the synthesis of aryl esters using Ni catalysts, including thermal,^{15,21} electrochemical,²² dual photocatalytic,^{13,14,23–28} semi-heterogeneous¹⁴ and single-atom (heterogeneous) photocatalytic²⁹ protocols. Moreover, most documented examples are limited in substrate scope, primarily focusing on aryl iodides,^{16,30} or require elevated temperatures.³¹

Since 2017, several reports have detailed the nickel-catalyzed arylation of carboxylates (Fig. 1).^{13–15} The group led by MacMillan described that Ni-bipyridine catalysts can facilitate visible-light-driven esterification reactions using an iridium complex as photosensitizer.¹³ Pieber and Seeberger have used a semi-heterogeneous system combining graphitic carbon nitride photocatalysts and nickel complexes for the C–O coupling reaction.^{13,14} In addition, Tosoni, Vilé and co-workers recently reported that a Ni atom-supported carbon nitride material effectively catalyzes cross-coupling of carboxylic acids and alkyl halides.²⁹ In early 2020, Nocera and co-workers demonstrated that photoredox-like amination, etherification, and esterification of aryl bromides can be achieved in the dark using a Ni(II)/dtbbpy catalyst in conjunction with zinc as a sacrificial reductant, supporting the hypothesis of a thermally driven catalytic cycle.¹⁵ Additionally, there are a few reports where nickel

^aUniversity of Regensburg, Institute of Inorganic Chemistry, 93040 Regensburg, Germany. E-mail: rafael.rodriguez@iccm.cnr.it; robert.wolf@chemie.uni-regensburg.de

^bCenter for Catalytic Hydrocarbon Functionalizations, Institute for Basic Science (IBS), Daejeon, 34141, Republic of Korea

^cUniversity of Regensburg, Institute of Physical and Theoretical Chemistry, 93040 Regensburg, Germany

^dDepartment of Chemistry, Korea Advanced Institute of Science and Technology (KAIST), Daejeon, 43141, Republic of Korea. E-mail: mbaik2805@kaist.ac.kr

† Electronic supplementary information (ESI) available: Synthetic and catalytic experimental procedures, detailed spectral and crystallographic characterization, DFT calculations. CCDC 2354527–2354534. For ESI and crystallographic data in CIF or other electronic format see DOI: <https://doi.org/10.1039/d4sc04257c>

‡ Current (permanent) address: Istituto di Chimica dei Composti Organometallici, Consiglio Nazionale delle Ricerche, Via Madonna del Piano 10, Sesto Fiorentino, 50019, Italy.

§ Current address: Department of Chemistry, Johannes Gutenberg University, Duesbergweg 10-14, 55128 Mainz, Germany.

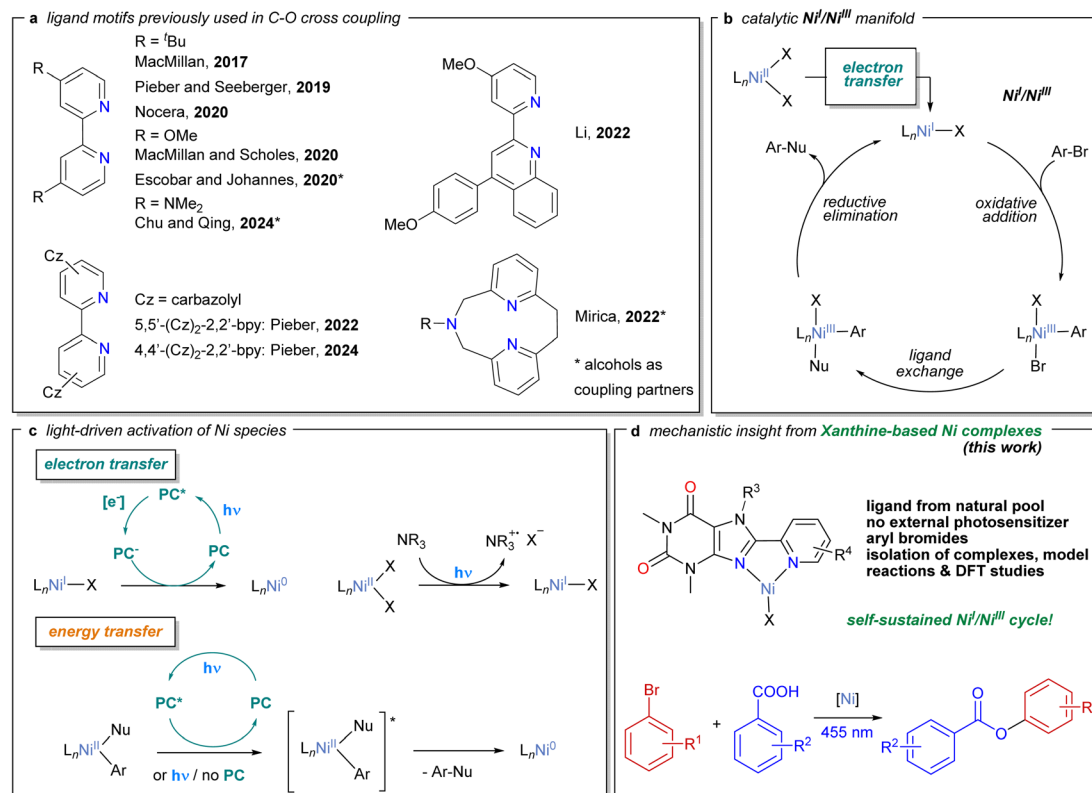


Fig. 1 (a) Ligands previously used in C–O cross-couplings, (b) proposed Ni(I)/Ni(III) mechanism for dual Ni-bpy-catalyzed C–O cross-couplings, (c) principal Ni catalyst activation modes, (d) C–O cross-couplings catalyzed by xanthine-based Ni species.

catalysts are employed without external photosensitizers.³¹ A photoactive bipyridine-like ligand, which combines substituted quinoline and pyridine motifs, has been used for various metallaphotoredox cross-coupling reactions as described by Li and co-workers.¹⁶ The Pieber group introduced carbazole-decorated bipyridine ligands, Czbp (Czbp = 5,5'-dicarbazolyl-2,2'-bipyridyl and 4,4'-dicarbazolyl-2,2'-bipyridyl), that promote intraligand charge transfer to activate the nickel catalyst.^{30,32} Recently, Mirica and co-workers developed a single nickel catalyst for C–O cross-coupling reactions using a tridentate pyridinophane ligand.³³ These advancements in single-metal photoredox catalysts have significantly enhanced the utility of metallaphotoredox catalysis in C–O cross-coupling reactions.^{1,16,34}

The mechanism of Ni-catalyzed cross-coupling reactions has been debated in recent literature. Most studies focused on the Ni-bipyridine catalyst system for which several viable catalytic manifolds have been proposed, involving Ni(I)/Ni(III), Ni(0)/Ni(II) and Ni(0)/Ni(II)/Ni(III)/Ni(I) cycles.^{12,32,33,35–38} From these studies, it has emerged that a Ni(I)/Ni(III) cycle likely operates in most dual Ni-bipyridine-catalyzed C–E cross-couplings (E = C, O, S; Fig. 1b).^{15,32,39–44} Here, the (light-driven) reduction of the Ni(II) precursor to the catalytically competent Ni(I) species initiates the catalytic cycle, comprising individual steps that are accessible without the involvement of photochemical events. Several studies showed that oxidative addition to Ni(I) polypyridine complexes is thermally accessible.^{33,39–42,45} Van der Veen,

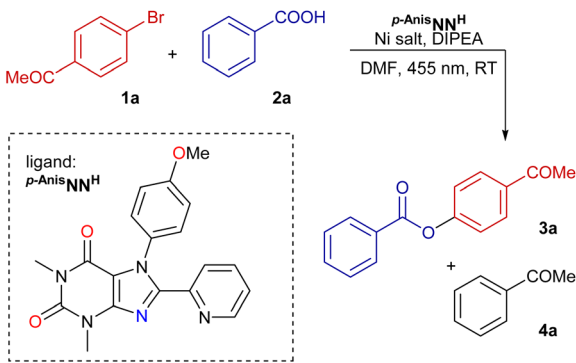
Thomas, and Pieber suggested that direct photoactivation of a Ni(II)-halide complex generates the Ni(I) counterpart. These authors showed that the catalytic Ni(I)/Ni(III) cycle can be initiated by a visible-light-induced homolysis (VLIH).^{30,46–48} Moreover, synthetic mechanistic studies by Mirica and co-workers suggest a thermal Ni(I)/Ni(III) mechanism in the single Ni-catalyzed etherification of aryl bromides.³³ In 2023, Bahamonde and co-workers presented mechanistic evidence of a Ni(0)/Ni(II)/Ni(III) cycle for heterogeneous Ni-photoredox amide arylation reactions.⁴⁹ Recently, the Pieber group suggested the involvement of a Ni(I)/Ni(III) cycle in C(sp²)-C(sp³) cross-coupling reactions.³² Although the Ni(I)/Ni(III) cycle seemingly operates in many reported protocols, the determination of a specific catalytic mechanism is intricate for any new catalyst system. Indeed, it has been noted by Hadt and co-workers that the population of a specific catalyst manifold is governed by the electronic structure of the Ni catalysts,¹² which is highly dependent on the chemical environment of the metal atom and especially the ligands.⁴³ Therefore, the mechanism of Ni-catalyzed cross-couplings must be examined case by case. Previous studies have considered several catalyst activation modes (Fig. 1c). In dual photocatalytic systems, one-electron reduction of Ni(II) complexes may generate reactive Ni(0) species capable of undergoing oxidative addition with aryl halides.³⁷ Pieber and Seeberger demonstrated that light irradiation can produce photoexcited Ni(II)* species, facilitating the product's reductive elimination.²⁷ In addition, Hess described



the photochemical reduction of Ni(II) complexes by amines, presenting an alternative light-driven electron transfer process for activating Ni complexes that does not require an additional photocatalyst.^{50,51}

In this study, we demonstrate that the combination of fluorescent C8-pyridyl xanthenes and Ni(II) salts facilitates the light-driven *O*-arylation of carboxylates, specifically using xanthine derivatives such as N7-substituted theophylline or caffeine. Xanthenes are appealing scaffolds because they are naturally abundant compounds found in edible products such as coffee, tea, and chocolate. By chemically modifying the xanthine backbone, it is possible to create bidentate ligand motifs that serve as luminescent molecules.^{52,53} Our findings indicate that these xanthine-based nickel complexes act as effective catalysts in the light-driven *O*-arylation of carboxylates. To understand how this xanthine-based nickel system functions, we conducted a mechanistic investigation using both experimental and computational techniques. We reveal the coordination behavior and photophysical properties of selected ligands and complexes, which include the isolation and crystallographic characterization of pyridyl-xanthine Ni(I) complexes. Density Functional Theory (DFT) calculations provide essential insights into the mechanistic pathways, suggesting that a thermally accessible Ni(I)/Ni(III) cycle is involved. This cycle is initiated by the light-promoted reduction of the Ni(II) precursor complexes.

Table 1 Coupling reaction between 4'-bromoacetophenone (**1a**) and benzoic acid (**2a**)^a

					
Entry	Metal salt	Ligand	3a ^b (%)	4a ^b (%)	Sel. ^b 3a : 4a
1 ^c	Ni(OTf) ₂	<i>p</i> -AnisNNH	64	32	2.00
2	NiBr ₂	<i>p</i> -AnisNNH	52	35	1.49
3	Ni(OTf) ₂	dtbbpy	30	20	1.50
4	Ni(OTf) ₂	None	15	12	1.25
5	None	<i>p</i> -AnisNNH	—	39	—
6 ^d	Ni(OTf) ₂	<i>p</i> -AnisNNH	n.d.	n.d.	—

^a Standard conditions: 4-bromoacetophenone (39.9 mg, 0.20 mmol), benzoic acid (48.9 mg, 0.40 mmol, 2 equiv.), Ni salt (10.0 μmol, 5 mol%), *p*-AnisNNH (72.0 mg, 20.0 μmol, 10 mol%), DIPEA (142 μL, 0.81 mmol, 4 equiv.), DMF (0.50 mL, 0.4 mM), 18 h, 40 °C, blue LED (455 nm, 7.0 W, photoreactor TAK 120). ^b Yield and selectivity (sel.) determined by GC-FID using 1,3,5-trimethoxybenzene as internal standard (8.4 mg, 0.05 mmol) and an appropriate calibration curve. ^c Average of five independent runs. ^d No light irradiation. dtbbpy = 4,4'-di-tertbutyl-2,2'-bipyridine.

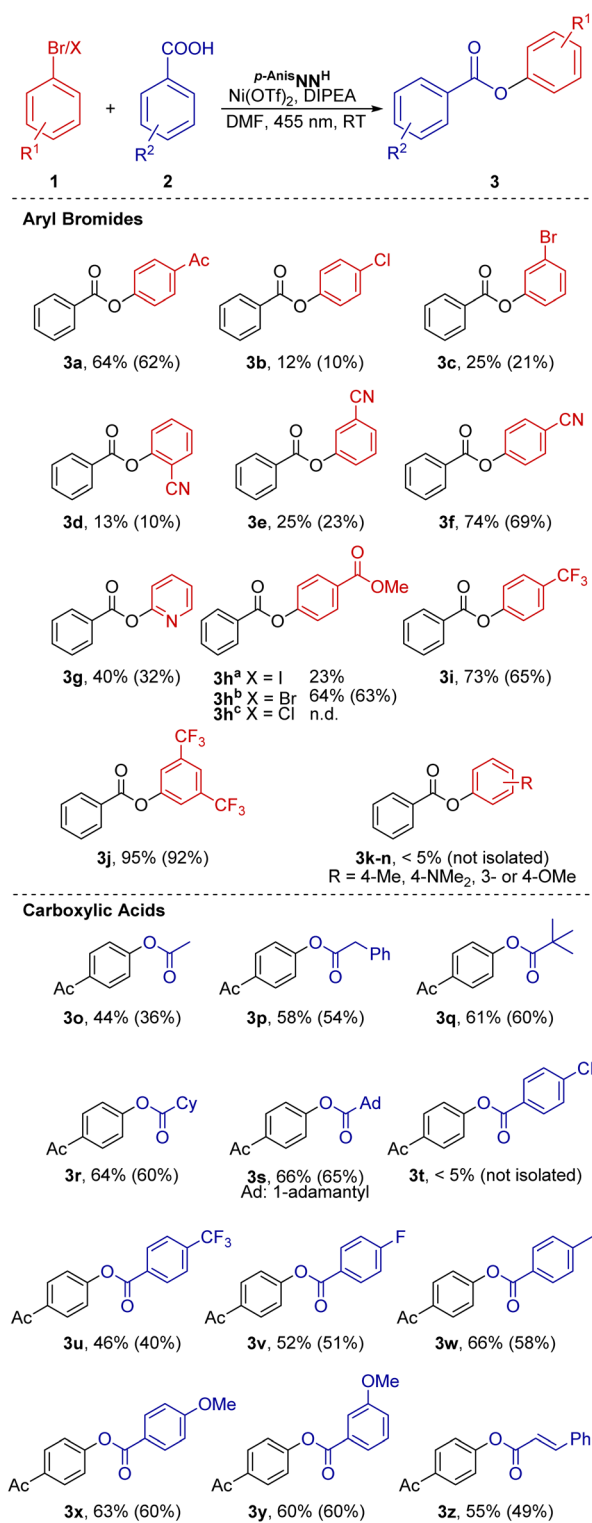


Fig. 2 Substrate scope for the nickel catalyzed arylation of carboxylates. Conditions: aryl bromide (0.20 mmol), carboxylic acid (0.40 mmol, 2 equiv.), Ni(OTf)₂ (3.6 mg, 10.0 μmol, 5 mol%), *p*-AnisNNH (7.2 mg, 20.0 μmol, 10 mol%), *N,N*-diisopropylethylamine (DIPEA) (142 μL, 0.81 mmol, 4 equiv.), DMF (0.50 mL, 0.4 mM), 18 h, 40 °C, blue LED (455 nm, 7.0 W, photoreactor TAK 120). Yields were determined by GC-FID. Yields of isolated product are given in parentheses.

Results and discussion

Photocatalytic cross-coupling of carboxylates and aryl halides

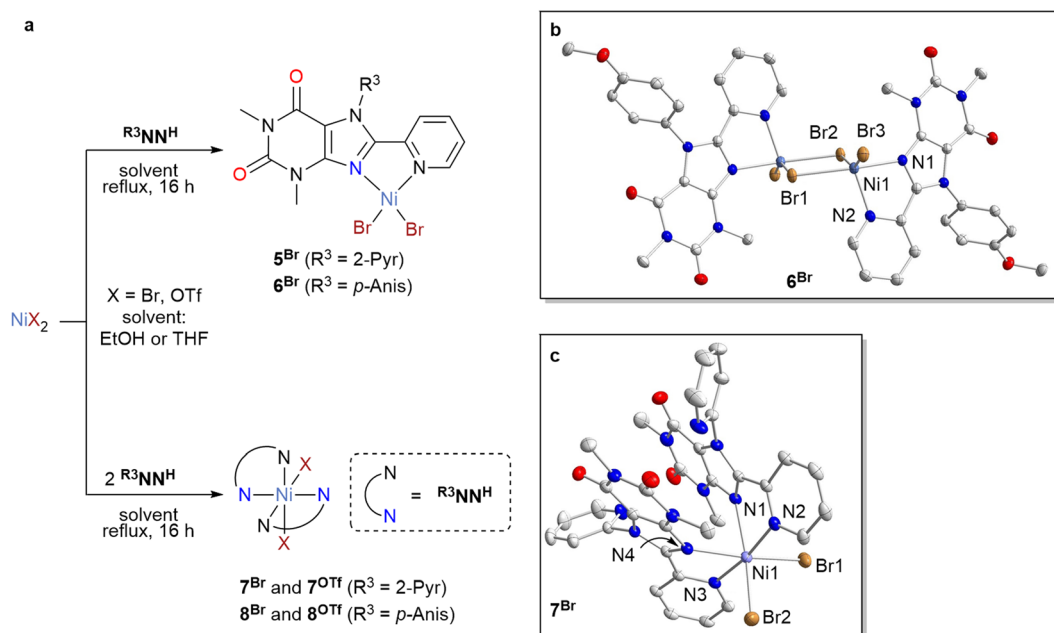
A library of several C8-pyridyl xanthine chelate ligands was prepared by modification of established procedures (see ESI† for detailed information†).^{52,54–56} The synthesized ligands and simple Ni(II) salts were used as *in situ* generated Ni(II) catalysts, which enabled photocatalytic cross-coupling of 4'-bromoacetophenone (**1a**) with benzoic acid (**2a**) (Table 1). Among the ligands tested, the *para*-anisyl substituted xanthine derivative *p*-Anis^{6Me}NN^H (entry 1, *p*-Anis = *p*-(OCH₃)-C₆H₄) was most efficient, surpassing the yield and selectivity of 4,4'-di-*tert*-butyl-2,2'-bipyridine (dtbbpy) which is commonly used for nickel photocatalysis (Table 1, entry 3).¹ Typically, alkyl substituents on the N7 atom of the xanthine scaffold, R³ = Me, ¹Pr and Bn, yielded either low catalytic activity or poor selectivity (Table S3, entries 1–4†). In general, aromatic substituents on the xanthine unit, R³ = C₆H₅, 2-C₅H₄N, 4-OCH₃-C₆H₄, allowed for high conversions (Table S3, entries 5–8†) except for ligands *p*-Anis^{6Me}NN^H and *p*-OHPh^{6Me}NN^H (Table S3, entries 9 and 10†), that gave rise to moderate conversions. The reaction selectivity varies depending on the nature of the aromatic ring on the xanthine N7 atom, with *p*-OMe or *p*-OH exhibiting the best product/side product ratios (Table S3, entries 8 and 10†).

Control reactions showed that the lack of an exogenous ligand resulted in a diminished conversion and poor selectivity (Table 1, entry 4). Cross-coupling was not observed in the absence of nickel or without irradiation (Table 1, entries 5 and 6). Details of the optimization steps under different reaction

conditions are provided in the ESI†, including the evaluation of the effect of incorporating some common external photosensitizers (Table S2†).

Considering the results obtained in the initial evaluation, we expanded the scope of the reaction to test a range of substrates under the optimized reaction conditions (Fig. 2). Substrates featuring electron-withdrawing groups (EWG) at the *o*- or *p*-positions on aryl bromide **1** furnished good product yields (64–74%) (products **3a**, **3f**, **3h**, **3i**). The 3,5-(CF₃)₂-substituted product **3j** was obtained in 95% yield. In contrast, substrates with EWGs at the *m*-position (Br, **3c**; CN, **3e**) or a heterocyclic substituent (2-py, **3g**) afforded low to moderate yields (25–40%). A halide atom (Cl) in *p*-position resulted in a low yield (12%). Similarly, CN substitution at the *o*-position significantly reduced the catalytic activity (**3d**, 13%). Aryl bromides bearing electron-donating groups proved unsuitable as coupling partners for benzoic acid (**3k–n**). Aryl iodides (**3h^a**) also showed lower product yields, with an increased formation of the dehydrohalogenation product (**4h**). Aryl chlorides did not undergo the desired transformation (**3h^c**).

We also screened a series of carboxylic acids **2**. Aliphatic R² substitution of **2** led to moderate yields (44–66%) for aryl esters **3o–s**. The use of electron-poor benzoic acids did not significantly influence the product yield. Whereas moderate improvements were observed for compounds **3u** and **3v**, with yields of 46% and 52%, respectively, the cyano-substituted substrate **3t** resulted only in trace amounts of the product. Electron-rich carboxylic acids provided the respective esters in moderate yields, **3w–z** (55–66%).



Scheme 1 (a) General synthesis of xanthine-based Ni(II) complexes [NiBr₂(R³NN^H)] (5Br/6Br) and [NiX₂(R³NN^H)₂] (7/8) with solid-state molecular structures of (b) [NiBr₂(μ-Br)(*p*-Anis^{6Me}NN^H)]₂ (6Br), and (c) [NiBr₂(pyr^{6Me}NN^H)]₂ (7Br). Displacement ellipsoids are drawn at the 50% probability level. H-atoms have been omitted for clarity. Selected bond lengths [Å] and angles [°] for (6Br): Ni–N1 2.052(3), Ni–N2 2.013(3), Ni–Br1 2.4875(7), Ni–Br2 2.5549(7), Ni–Br3 2.4113(7), N1–Ni–N2 80.25(11), N1–Ni–Br1 167.94(9), Br1–Ni–Br3 94.59(2), Br2–Ni–Br3 154.45(3); for 7Br: Ni1–N1 2.284(2), Ni1–N2 2.059(2), Ni1–N3 2.065(2), Ni1–N4 2.244(2), Ni1–Br1 2.504(1), Ni1–Br2 2.500(1), N1–Ni1–N2 76.72(7), N3–Ni1–N4 76.96(7), Br1–Ni1–Br2 100.11(2).



Synthesis and characterization of catalytically relevant species

The coordination behavior of the most effective ligands in the catalytic transformation described above, PyrrNN^{H} and $p\text{-AnisNN}^{\text{H}}$, was investigated towards $\text{Ni}(\text{OTf})_2$ and NiBr_2 (Scheme 1). Both ligands form stable and isolable 1 : 1 complexes $[\text{NiBr}_2(\text{R}^3\text{NN}^{\text{H}})]_2$ (5^{Br} , $\text{R}^3 = 2\text{-pyr}$; 6^{Br} , $\text{R}^3 = p\text{-Anis}$), as well as 2 : 1 complexes $[\text{NiBr}_2(\text{R}^3\text{NN}^{\text{H}})]_2$ (7^{Br} , $\text{R}^3 = 2\text{-pyr}$; 8^{Br} , $\text{R}^3 = p\text{-Anis}$) with NiBr_2 , depending on the ligand stoichiometry used in the synthesis. In the solid state, complex 6^{Br} adopts a bromide-bridged dimeric structure featuring five-coordinate Ni^{2+} cations, comprising one bidentate C8-pyridyl xanthine chelate and three bromide ligands (see Scheme 1b). Notably, the solution ^1H -NMR spectra of complexes 5^{Br} and 6^{Br} exhibited paramagnetically shifted signals (see the ESI for details[†]).

In addition, we isolated 2 : 1 complexes $[\text{Ni}(\text{OTf})_2(\text{R}^3\text{NN}^{\text{H}})]_2$ (7^{OTf} , $\text{R}^3 = 2\text{-pyr}$; 8^{OTf} , $\text{R}^3 = p\text{-Anis}$). Complexes 7 and 8 feature hexacoordinate $\text{Ni}(\text{II})$ centers with *cis*-configuration in the solid state (Scheme 1). In solution, these octahedral $\text{Ni}(\text{II})$ complexes are NMR silent.

To investigate the possible role of the synthesized complexes in the catalytic arylation of carboxylates under study, we explored the photoreduction of the $\text{Ni}(\text{II})$ compounds. In this regard, we measured the UV-vis absorption spectra of the individual reaction components in the catalysis. Weak d-d transitions were observed in the visible spectrum of the hexacoordinated $[\text{Ni}(\text{DMF})_6]^{2+}$ ($^3\text{A}_{2g} \rightarrow ^3\text{T}_{1g}(\text{F})$, $^1\text{E}_g$: 700–780 nm; $^3\text{A}_{2g} \rightarrow ^3\text{T}_{1g}(\text{P})$: 410 nm, Fig. S7 in the ESI[†]). None of the other components of the reaction mixture absorb light in the spectral range around 450 nm. Nevertheless, we found significant changes in the absorption spectra of the mixtures of NiBr_2 or $[\text{NiBr}_2(p\text{-AnisNN}^{\text{H}})]$ (6^{Br}) with *N,N*-diisopropylethylamine (DIPEA) in DMF after irradiation with blue LED light (455 nm). The resulting spectra showed increased absorption in the spectral regions 370–490 nm and 490–590 nm (Fig. 3). While the absorption below 400 nm stems from $p\text{-AnisNN}^{\text{H}}$ (Fig. S4 in the ESI[†]), the new absorption band at 370–490 nm can presumably be attributed to the decomposition of *N,N*-diisopropylethylamine radical cation ($\text{DIPEA}^{+\bullet}$) and its reaction with Ni

complexes.⁵⁷ The absorption bands between 490–590 nm are likely associated with the formation of $\text{Ni}(\text{I})$ species (*vide infra*).

To gain further insight into this matter, we also prepared low-valent $\text{Ni}(\text{I})$ and $\text{Ni}(\text{0})$ complexes with the ligand $p\text{-AnisNN}^{\text{H}}$ (Scheme 2). Commercially available $[\text{Ni}(\text{cod})_2]$ (**9**; cod = 1,5-cyclooctadiene) was subjected to ligand exchange with $p\text{-AnisNN}^{\text{H}}$ (see ESI for details[†]). Unfortunately, all efforts to isolate and characterize the putative complex $[\text{Ni}(\text{cod})(p\text{-AnisNN}^{\text{H}})]$ (**10**) were unsuccessful, possibly due to its high sensitivity to temperature and light. In fact, the reaction mixture forms metallic mirrors alongside the free ligands $p\text{-AnisNN}^{\text{H}}$ and 1,5-COD above -30°C or when exposed to daylight.

To confirm the formation of **10**, the related $\text{Ni}(\text{I})$ compound $[\text{NiBr}(p\text{-AnisNN}^{\text{H}})]$ (**11^{Br}**) was synthesized in two steps from **9**. The *in situ* generated complex **10** was treated with 1 equiv. of complex 6^{Br} to access **11^{Br}** via comproportionation. Complex **11^{Br}** forms a precipitate that is insoluble in common organic solvents. Thus, characterization by solution NMR and single-crystal XRD analysis were not viable. The precipitate results from the formation of halide-bridged dimers of complex **11^{Br}**. Of note, similar precipitates were reported for $\text{Ni}(\text{I})$ complexes with bipyridine (bpy) and phenanthroline (phen) ligands.^{40,42,44,45,58–60} DFT simulations by Hadt on dimeric dtbbpy

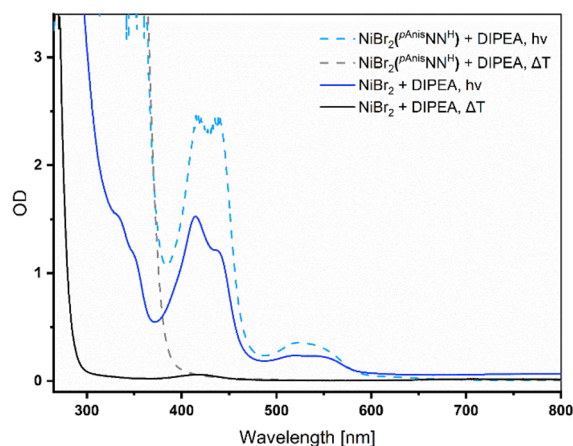
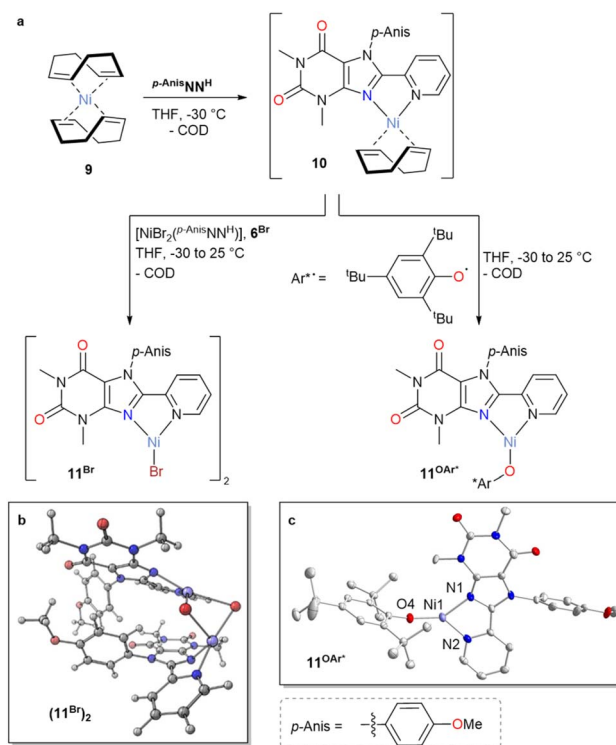


Fig. 3 UV-vis absorption spectra of NiBr_2 (20 mM) with DIPEA (1.6 M, 80 equiv.) or 6^{Br} with DIPEA (1.6 M, 80 equiv.) after thermal reaction at 65°C (ΔT), and after 18 h of illumination at 455 nm (*hν*), respectively.



Scheme 2 (a) Synthesis of low valent Ni species $[\text{Ni}(\text{cod})(p\text{-AnisNN}^{\text{H}})]$ (**10**) and $[\text{NiX}(p\text{-AnisNN}^{\text{H}})]$ ($\text{X} = \text{Br}$ (**11^{Br}**), OAr^* (**11^{OAr*}**)), starting from the precursor $[\text{Ni}(\text{cod})_2]$ (**9**). (b) Structure of the dimer (**11^{Br}**)₂ calculated with DFT. (c) Solid-state molecular structure of **11^{OAr*}**. Displacement ellipsoids are drawn at the 40% probability level. H-atoms have been omitted for clarity. Selected bond lengths [Å] and angles [°]. Ni–N1 1.975(3), Ni–N2 1.935(3), Ni–O4 1.819(7), C10–N2 1.366(4), C1–C2 1.463(4), C8–N1 1.349(4), N1–Ni–N2 82.21(11), N1–Ni–O4 140.59(9), N2–Ni–O4 136.84(8).

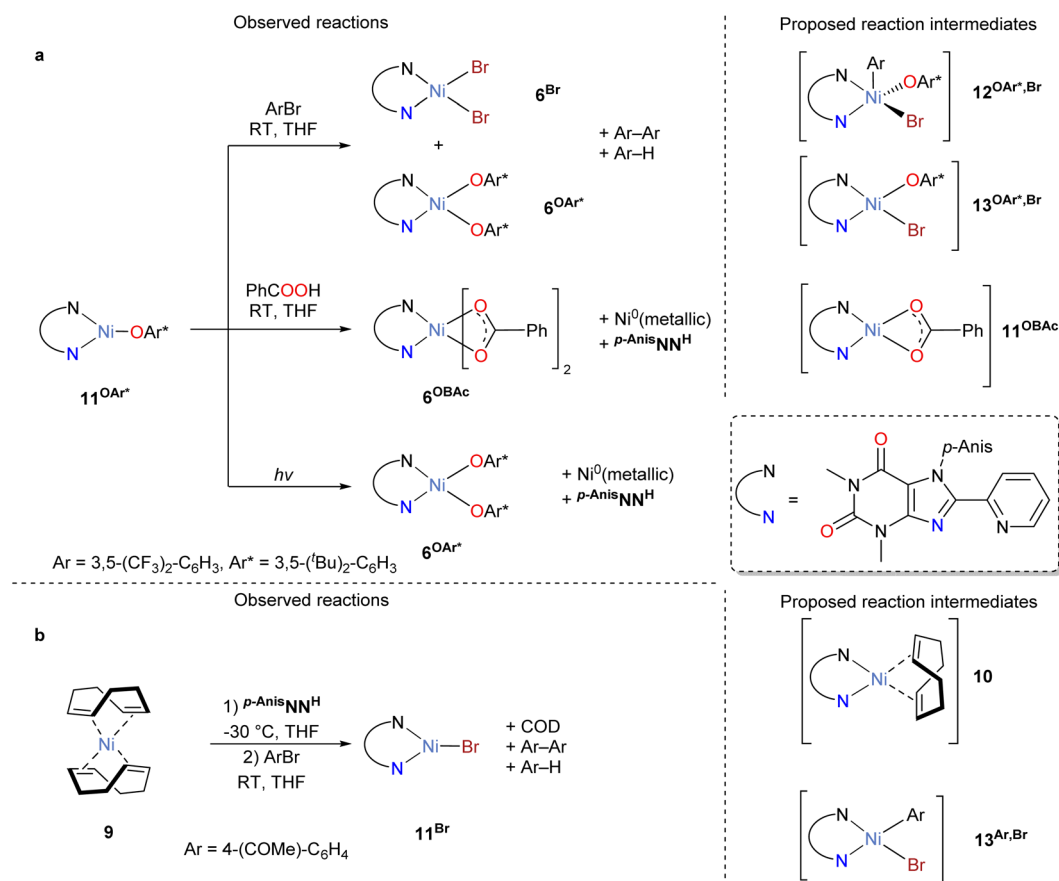
complexes of Ni(II) found bent and flat dimer structures with similar energies.⁴⁵ To better understand the formation of this kind of species in our case, we performed DFT calculations on the structure of dimer (**11^{Br}**)₂. According to these, (**11^{Br}**)₂ exists only as a severely bent structure (spin state *S* = 1, Scheme 2b). We also found that the dimer formation is energetically uphill by $\Delta G = 11.2 \text{ kcal mol}^{-1}$ in solution phase. Interestingly, the dimerization is exergonic in gas-phase ($\Delta G = -8.7 \text{ kcal mol}^{-1}$ and $\Delta H = -1.3 \text{ kcal mol}^{-1}$), suggesting that the precipitation of the compound is the driving force behind the dimerization.

An aryloxy substituted complex, [Ni(OAr*)(*p*-AnisNNH)] (**11^{OAr*}**, Ar* = 2,4,6-(*t*-Bu)₃-C₆H₂), closely related to **11^{Br}**, was accessed by treating a mixture of [Ni(cod)₂] (**9**) and *p*-AnisNNH with the aryloxy radical [•]OAr*.⁶¹ In contrast to **11^{Br}**, complex **11^{OAr*}** is soluble in most common organic solvents. The ¹H-NMR spectrum exhibits broad high-field shifted signals typical of a paramagnetic species. The molecular structure of **11^{OAr*}** was determined by single-crystal X-ray diffraction (Scheme 2c). The N=C=C=N scaffold of the ligand backbone (C–N 1.349(4) and 1.366(4) Å, C–C 1.463(4) Å) remains unaltered relative to the free ligand *p*-AnisNNH (C–N 1.344(2) Å and 1.342(2) Å, C–C 1.471(2) Å). These findings indicate that the ligand is not reduced.

The UV-vis spectrum of **11^{OAr*}** supports our initial assignment that the bands between 490–590 nm observed in the

photoreduction of the Ni(II) compounds correspond to possible Ni(I) species. In fact, a significant absorption between 400–600 nm was present in the UV-vis spectrum of **11^{OAr*}** (Fig. S7 in the ESI†). Moreover, UV-vis monitoring of a diluted and freshly prepared solution of **11^{Br}**, obtained *in situ* by treating [Ni(cod)₂] with *p*-AnisNNH and 4-Br-C₆H₄-COMe, as shown in Scheme 3a (*vide infra*), revealed two small absorption bands at 470 and 520 nm (Fig. S10 in the ESI†). Once formed, the isolated material is insoluble in common organic solvents, probably due to the formation of the halide-bridged dimer (**11^{Br}**)₂ (*vide supra*), hence hampering the measurement of its absorption spectrum. Furthermore, the reduction of NiBr₂ with Zn was previously reported to result in increased absorption between 500–600 nm.²¹

Additionally, and within our theoretical calculations (using DFT), we explored possible pathways for the reduction of Ni(II) (Scheme S11 in the ESI†). The spectroscopic observations and DFT calculations are consistent with the photoreduction of Ni(II) by DIPEA, proceeding initially to a Ni(I) species *via* light-induced single electron transfer (SET). The photoreduction most likely results from a Ni²⁺-centered d–d transition. Further reduction to Ni(0) species can occur as a side reaction. However, our calculations show that these unstable Ni(0) complexes undergo disproportionation with Ni(II) to Ni(I) (see Scheme S11†).



Scheme 3 (a) Oxidative addition of ArBr and transmetalation with benzoic acid from Ni(II) complex **11^{OAr*}** as well as decomposition from irradiation. (b) Oxidative addition of ArBr to Ni(0) complex **10**.

Finally, our efforts to isolate and characterize Ni(III) compounds bearing the ligand $p\text{-AnisNN}^{\text{H}}$ have been unsuccessful to date (*vide infra* and see ESI†).

Synthetic model reactions

Once the low-valent nickel species **10** and **11**^{OAr*} were identified, and **11**^{OAr*} was characterized, we tried to understand whether the Ar–Br bond in the aryl halide substrate can be activated under thermal conditions. In this regard, we examined the oxidative addition of aryl bromide ArBr to the *in situ* generated species **10** and to complex **11**^{OAr*}. By treating **11**^{OAr*} with ArBr (Ar = 3,5-(CF₃)₂-C₆H₃), we observed the formation of [NiBr₂($p\text{-AnisNN}^{\text{H}}$)] (**6**^{Br}) and [Ni(OAr*)₂($p\text{-AnisNN}^{\text{H}}$)] (**6**^{OAr*}) alongside Ar–Ar and Ar–H (Scheme 3a). The formation of Ar–Ar and Ar–H was detected by ¹⁹F-NMR spectroscopy. This is consistent with the oxidative addition of ArBr to **11**^{OAr*} forming intermediate **12**^{OAr*,Br}, followed by Ni–Ar bond homolysis to **13**^{OAr*,Br} and ligand exchange of the complexes. Alternatively, the presumed Ni(III) species **12**^{OAr*,Br} can comproportionate with **11**^{OAr*} forming Ni(II) compounds. Upon ligand redistribution, reductive elimination from the assumed binary complex [Ni(Ar)₂($p\text{-AnisNN}^{\text{H}}$)] (**6**^{Ar}) would lead to Ar–Ar, while HAT from DIPEA⁺⁺ to any Ni–Ar species will lead to Ar–H. Further evidence of the Ni–Ar bond homolysis was obtained by treating the Ni(II) complex [Ni(Ar)Br(PPh₃)₂] (**14**) with $p\text{-AnisNN}^{\text{H}}$ (one equiv.), affording the Ni(I) complex [NiBr($p\text{-AnisNN}^{\text{H}}$)(PPh₃)₂] (**11**^{Br}·PPh₃), which was isolated and characterized by ¹H-NMR spectroscopy and single crystal XRD analysis (see the ESI for further details†).

Similarly, upon treatment of the *in situ* generated Ni(0) complex **10** with 4-bromoacetophenone (Scheme 3b), the Ni(I) complex **11**^{Br} was formed along with the biphenyl (Ar–Ar) and the hydrodehalogenation (Ar–H) side products (Ar = 4-(COMe)-C₆H₄). The formation of Ar–Ar was observed by GC-MS analysis of the reaction mother liquor and confirmed by ¹H- and ¹³C{¹H}-NMR spectroscopy (see Scheme S8 and Fig. S83 in the ESI†). Likely, Ni–Ar bond homolysis took place, thus reducing Ni(II) to Ni(I), as reported by Doyle.⁴⁷ Again, another scenario to explain this reactivity would be the comproportionation of the presumed Ni(II) species [Ni(Ar)(Br)($p\text{-AnisNN}^{\text{H}}$)] with **10**, thus forming Ni(I) compounds.

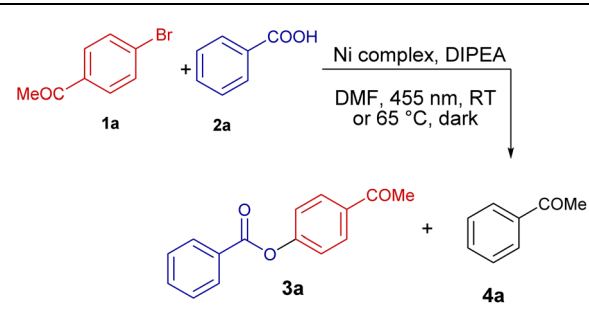
Our synthetic studies therefore suggested that low-valent nickel species **10** and **11**^{OAr*} can activate the Ar–Br bond under thermal conditions. Additionally, we treated **11**^{OAr*} with PhCOOX (X = H, K) to simulate the transmetalation reaction. Instead of the putative Ni(I) complex [Ni(O(CO)Ph)($p\text{-AnisNN}^{\text{H}}$)] (**11**^{OAc}), the Ni(II) complex [Ni(O(CO)Ph)₂($p\text{-AnisNN}^{\text{H}}$)] (**6**^{OAc}) was formed alongside a metallic mirror of Ni(0). This indicates a disproportionation of the Ni(I) species **11**^{OAc} driven by precipitation of Ni(0). Disproportionation can also be observed when irradiating complex **11**^{OAr*} with blue light. These results underline the susceptibility of the Ni(I) and Ni(III) species towards deactivation *via* comproportionation, driven either thermally or by light.

Furthermore, we aimed to identify viable catalytic intermediates among the abovementioned Ni species. Specifically, we repeated the cross-coupling of benzoic acids with aryl bromides

using stoichiometric amounts of the nickel complexes obtained in different formal oxidation states. Complexes **6**^{Br}, **10** and **11**^{OAr*} were reacted with **1a** in a 1 : 1 ratio, either under light irradiation (455 nm) or in the dark (thermally). The results are summarized in Table 2. Here, the cross-coupling reaction was not observed under thermal conditions (Table 2, entries 1, 3, 5), regardless of the nickel complex and its formal oxidation state. Instead, we observed hydrodehalogenation of **1a** promoted by Ni(0) and Ni(I) complexes (compounds **10** and **11**^{OAr*}, entries 1 and 3). Note that the Ni(II) complex **6**^{Br} was not able to produce cross-coupling or hydrodehalogenation product under thermal conditions (entry 5). However, substantial amounts of hydrodehalogenation product **4a** were formed under 455 nm LED light irradiation (entry 6). These findings agree with the reduction of **6**^{Br} to Ni(I) complex(es) under irradiation, that can promote hydrodehalogenation. Similarly, more hydrodehalogenation occurred in the presence of the Ni(0) species **10** under irradiation. Strikingly, we observed full conversion of the starting material and significant formation of the cross-coupling product **3a** for the reaction with complex **11**^{OAr*} under blue light irradiation (entry 4). The thermal process only delivered a relatively small amount of hydrodehalogenation (entry 3).

In conclusion, the model cross-coupling reactions show that only the Ni(I) species **11**^{OAr*} facilitates the *O*-arylation of benzoic acid **2a** with aryl bromide **1a**. The lack of product formation under thermal conditions with **11**^{OAr*} can be explained by the

Table 2 Cross-couplings mediated by stoichiometric amounts of Ni(0), Ni(I), and Ni(II) complexes under thermal and photochemical conditions^a



Entry	[Ni]	T	λ	3a ^b (%)	4a ^b (%)
1	Ni(0) 10 ^c	65 °C	—	—	70
2	Ni(0) 10 ^c	40 °C	455 nm	—	90
3	Ni(I) 11 ^{OAr*}	65 °C	—	—	21
4	Ni(I) 11 ^{OAr*}	40 °C	455 nm	50	50
5	Ni(II) 6 ^{Br}	65 °C	—	—	—
6	Ni(II) 6 ^{Br}	40 °C	455 nm	—	57

^a Conditions: 4-bromoacetophenone (3.9 mg, 20.0 μmol), benzoic acid (4.9 mg, 40.0 μmol, 2 equiv.), Ni species (20.0 μmol, 1 equiv.), DIPEA (14.2 μL, 80.0 μmol, 4 equiv.), DMF (0.50 mL, 0.04 mM), 18 h, 40 °C or 65 °C, blue LED (455 nm, operating power: 7.0 W, photoreactor TAK 120) or dark. ^b Yield and selectivity were determined by GC-FID using 1,3,5-trimethoxybenzene as internal standard (8.4 mg, 50.0 μmol). ^c Complex **10** was generated *in situ* by mixing [Ni(cod)₂] (20.0 μmol, 1 equiv.) and $p\text{-AnisNN}^{\text{H}}$ (200 μmol, 1 equiv.).



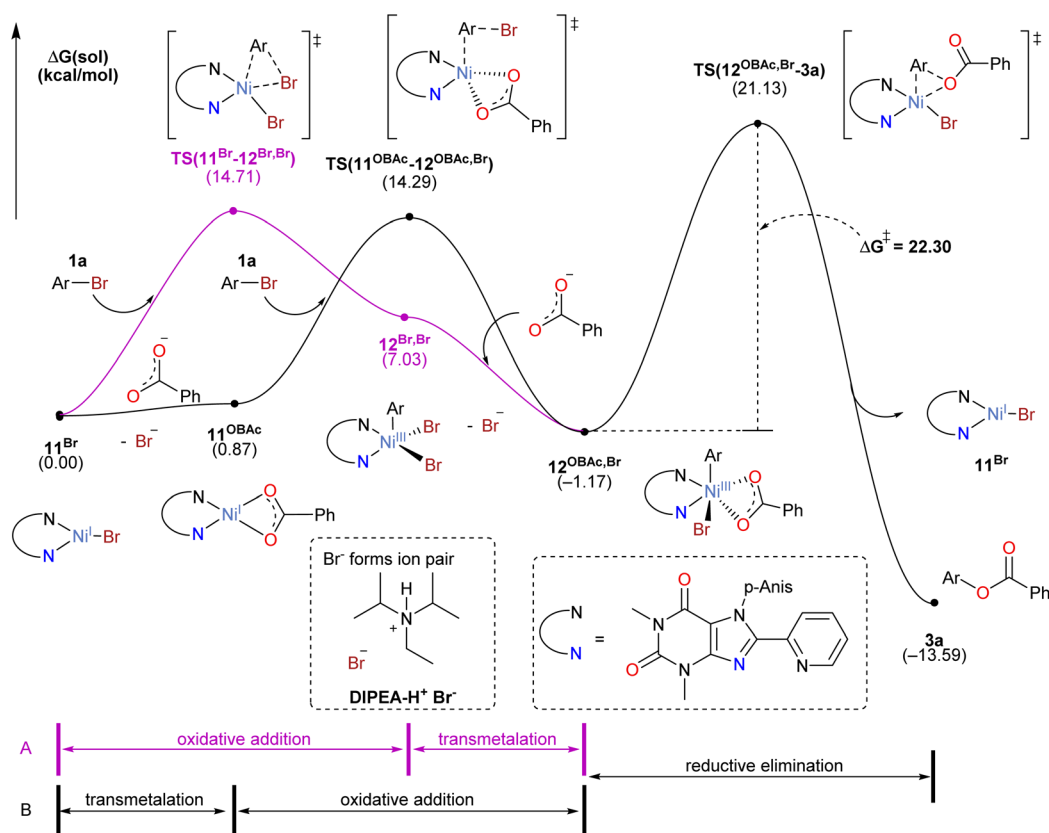
high concentration of Ni(I) species in the reaction mixture and a higher energy barrier for rate-limiting oxidative addition or reductive elimination steps compared to 11^{Br} (see Computational section). Ni(III) species formed by oxidative addition of aryl bromides are more likely to comproportionate with the abundant Ni(I) rather than following a productive reaction pathway under these conditions. Likewise, the same argument applies to the lack of product formation under photochemical conditions with 6^{Br} , in contrast with the catalytic experiment shown in Table 1, entry 2. Again, under the relatively high nickel concentration in the model stoichiometric reaction, the comproportionation of 11^{Br} and $12^{\text{X,Br}}$ (X = Br, OBAc) kinetically competes with the productive reaction step, the reductive elimination from Ni(III).

Computational investigations of the mechanistic pathway

The results obtained, including the isolation of possible catalytic intermediates, stoichiometric model reactions and UV-vis monitoring experiments, were taken into consideration to perform a detailed computational mechanistic investigation using density functional theory (DFT) calculations. This allowed for the construction of a complete catalytic cycle in atomistic detail, including all intermediate and transition state structures.

We performed DFT calculations to compare competing mechanistic pathways. Technical details of these calculations

are given in the ESI.† Scheme 4 shows the most plausible reaction energy profile of the proposed thermal catalytic cycle, which initiates from Ni(I) species 11^{Br} . We selected complex 11^{Br} as the model system for the calculations and compared two scenarios where either the oxidative addition of aryl bromide (path A) or the transmetalation of carboxylate (path B) initiates the catalytic cycle. We found that both pathways are equally viable. In path A, the oxidative addition of the aryl bromide to generate complex $12^{\text{Br,Br}}$ traverses a concerted transition state $\text{TS}(11^{\text{Br}}-12^{\text{Br,Br}})$, followed by the transmetalation of the carboxylate leading to $12^{\text{OBAc,Br}}$. Notably, ion pairing between a bromide anion and the cationic amine reductant ($\text{DIPEA-H}^+\text{Br}^-$)⁴³ facilitates the removal of the anion. In pathway B, the order of these steps is reversed: the transmetalation of carboxylate leads to 11^{OBAc} , followed by the oxidative addition $\text{TS}(11^{\text{OBAc}}-12^{\text{OBAc,Br}})$. The activation energies of the first steps of the two pathways are 14.7 and 14.3 kcal mol⁻¹ respectively. These energies suggest that both pathways are likely operative in parallel. These two initial steps result in a common Ni(III) intermediate $12^{\text{OBAc,Br}}$. The reductive elimination passes through a concerted transition state $\text{TS}(12^{\text{OBAc,Br}}-3\text{a})$, which is the most challenging transformation among the computed reaction steps, with an activation energy of 22.3 kcal mol⁻¹. This barrier is sufficiently low to enable a fast reaction under the experimental conditions, indicating that additional energy from photoexcitation is unnecessary for the elementary steps in the



Scheme 4 Core mechanism of the cross-coupling reaction. (A) Oxidative addition-first mechanism; (B) transmetalation-first mechanism. Ar = 4-(COMe)-C₆H₄.



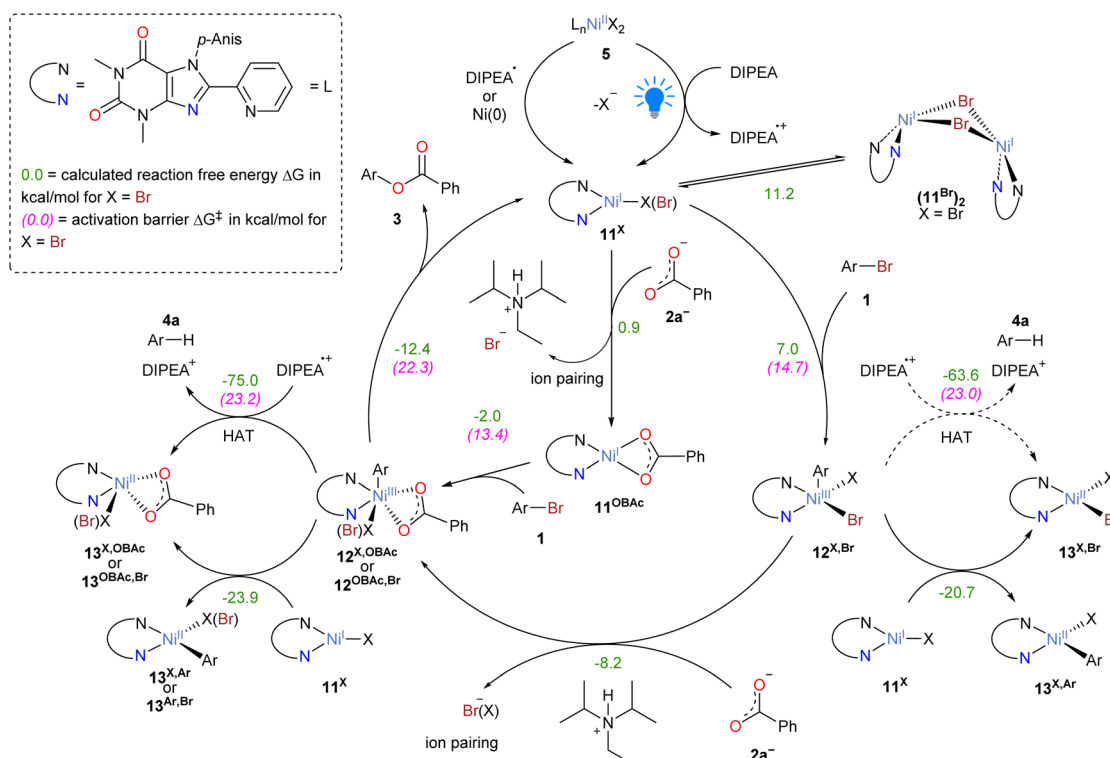
catalytic cycle. For instance, when the reaction is performed without irradiation, but using zinc powder as the sacrificial reductant instead, 25% of the *O*-aryl ester was obtained (Table S7, entry 8†). Moreover, only 15% of product was obtained using a liquid-cooled photoreactor, which keeps the reaction temperature at 18 °C (Table S7, entry 6†), in strong contrast with the 66% yield obtained at 40 °C (Table S7, entry 1†). This evidence is consistent with a significant contribution of thermally driven reaction steps to product formation. Notably, the Pieber group has recently reported a C–C cross-coupling system that operates through a Ni(I)/Ni(III) manifold, without involving photoredox reactivity, according to the mechanistic evidence.³²

Our calculations also explain the influence of the different counter-anions ($X = \text{Br}, \text{OTf}^-$ or OAr^{*-}) on the reaction (see Scheme S14 in the ESI†). The Ni(I) triflate complex OTf^- ($\mathbf{11}^{\text{OTf}}$) is readily converted into $\mathbf{11}^{\text{Br}}$, which is part of the core mechanism of the cross-coupling reaction (Scheme 4). When OAr^{*-} is used, the activation barrier of the oxidative addition ($\Delta G^\ddagger = 23.7 \text{ kcal mol}^{-1}$, Scheme S14c†) is higher than that of the reductive elimination commencing from $\mathbf{11}^{\text{Br}}$ ($\text{TS}(\mathbf{12}^{\text{OAc,Br}}-\mathbf{3a})$ in Scheme 4, $\Delta G^\ddagger = 22.3 \text{ kcal mol}^{-1}$). This barrier is consistent with the formation of cross-coupling product under blue-light irradiation (*vide supra*, Table 2 entry 4). The lacking success of the thermal reaction under the same conditions (Table 2 entry 3) is likely attributed to the rapid synproportionation of Ni(III) intermediates with $\mathbf{11}^{\text{OAr}^*}$ (*vide supra*).

The complete mechanism of Ni-catalyzed aryl esterification reaction is summarized in Scheme 5. The catalytic cycle is

initiated *via* the light-promoted reduction of Ni(II) complexes of the type $[\text{NiX}_2(\text{p-AnisNN}^{\text{H}})]$ ($X = \text{Br}, \text{OTf}^-, \text{OAr}^{*-}, \text{PhCOO}^-$) to Ni(I) complexes of the type $[\text{NiX}(\text{p-AnisNN}^{\text{H}})]$ ($\mathbf{11}^{\text{X}}$), which is described in detail in the ESI.† Starting from $\mathbf{11}^{\text{X}}$, two alternative mechanistic pathways are feasible. In the first scenario, $\mathbf{11}^{\text{X}}$ undergoes oxidative addition of aryl bromide forming the Ni(III) intermediate $\mathbf{12}^{\text{X,Br}}$. Subsequently, transmetalation with benzoic acid generates intermediate $\mathbf{12}^{\text{X,OAc}}$ or $\mathbf{12}^{\text{OAc,Br}}$. In the second scenario, the transmetalation takes place before oxidative addition, forming the benzoate complex $\mathbf{11}^{\text{OAc}}$. Then, oxidative addition of aryl bromide yields the same type of intermediate $\mathbf{12}^{\text{OAc,Br}}$. The catalytic cycle is closed by the reductive elimination of the cross-coupling product **3**, which regenerates the Ni(I) intermediate $\mathbf{11}^{\text{X}}$.

We note that Ni(III) species **12** can participate in side-reactions, which limit the selectivity and continuity of the catalytic processes (Scheme S13 in the ESI†). Our computational study suggests that $\mathbf{12}^{\text{OAc,Br}}$ can abstract a hydrogen atom from DIPEA^{*+} , with an activation energy of $\Delta G^\ddagger = 23.2 \text{ kcal mol}^{-1}$ ($\text{TS}(\mathbf{12}^{\text{OAc,Br}}-\mathbf{13}^{\text{OAc,Br}})$), indicating that hydrogen atom transfer (HAT) is thermally viable, but slower than the reductive elimination ($\Delta G^\ddagger = 22.3 \text{ kcal mol}^{-1}$, $\text{TS}(\mathbf{12}^{\text{OAc,Br}}-\mathbf{3a})$). As a result, the hydrodehalogenation side product **4** occurs as a side product in the catalytic reaction. It is also noted that the thermal activation of HAT from intermediate $\mathbf{12}^{\text{Br,Br}}$ is not feasible as the overall barrier of such reaction is $30.0 \text{ kcal mol}^{-1}$, associated with $\text{TS}(\mathbf{12}^{\text{Br,Br}}-\mathbf{6}^{\text{Br}})$.



Scheme 5 Complete mechanistic proposal of the visible-light-activated Ni-catalyzed *O*-arylation reaction. The energy unit is kcal mol^{-1} . $X = \text{Br}, \text{OTf}, \text{OAr}^*$.



In addition, comproportionation of Ni(III) species **12** with complex **11** results in catalytically inactive Ni(II) compounds. These Ni(II) species can reenter the catalytic cycle upon light-activated reduction. In fact, the redox couple Ni(II)/Ni(I) is reversible, as confirmed by cyclic voltammetry measurements with **11**^{OA}* (Fig. S84 in the ESI†). Furthermore, two complexes of type **11**^{Br} can be deactivated by the formation of a bent dimer (**11**^{Br})₂ as reported by Hadt.⁴⁵ The dimerization is uphill in energy ($\Delta G = 11.2 \text{ kcal mol}^{-1}$), but is driven by the precipitation of the insoluble dimer.

Conclusions

Xanthine-based chelate motifs can act as supporting ligands in nickel-catalyzed *O*-arylation of carboxylic acids with aryl bromides, achieving up to 95% product yields under blue light irradiation, while also facilitating the isolation of well-defined Ni(I) and Ni(II) complexes for mechanistic studies. Through UV-vis absorption spectroscopy and DFT calculations, we identified a thermally controlled Ni(I)/Ni(III) mechanism in C–O cross-coupling reactions. Furthermore, the sequence of the oxidative addition and transmetalation steps is variable and depends on the counter-ion present in the reaction. This observation may have implications for other Ni-catalyzed cross-coupling reactions. We also studied the hydrodehalogenation side-reaction and catalyst deactivation in our system. The computational investigations suggested that HAT using **DIPEA**^{•+} as the hydrogen atom source is a viable minor pathway. This might explain the hydrodehalogenation under our reaction conditions. In fact, the process has an activation energy similar to the reductive elimination of the cross-coupling product. Concerning catalyst deactivation, the comproportionation of Ni(I) and Ni(III) species generates inactive Ni(II) compounds which require reactivation by light-induced reduction.

DIPEA can play three possible independent roles in the catalytic cycle: First, it acts as a sacrificial reducing agent, producing Ni(I) species and generating the **DIPEA**^{•+} radical, which triggers HAT as a collateral effect. Second, **DIPEA** functions as a Brønsted base by deprotonating both the carboxylic acid and **DIPEA**^{•+} radical cation. Lastly, the protonated form of **DIPEA** (**DIPEA-H**⁺) facilitates the dissociation of Br[−] anions and enables transmetalation.

This study underscores the effectiveness of xanthine-based ligands in facilitating nickel-catalyzed C–O couplings. Notably, these ligands eliminate the need for an external photosensitizer and enable detailed mechanistic analyses. The combination of experimental and computational methods supports a mechanistic scenario in which the cross-couplings occur *via* a thermal mechanism, without requiring photochemical processes during the crucial reductive elimination step. Instead, visible light serves to sustain the thermal nickel(I)/nickel(III) cycle by regenerating the active nickel(I) species.

Data availability

The data supporting the findings of this study are available within the paper and its ESI† files. Crystallographic Information

Files (CIFs) have been deposited at the CCDC under the deposition numbers 2354527–2354534 (see ESI†). These data are provided free of charge by the joint Cambridge Crystallographic Data Centre and Fachinformationszentrum Karlsruhe Access Structures service.

Author contributions

Rafael E. Rodriguez-Lugo: conceptualization, investigation (synthetic, mechanistic and catalytic studies), writing – original draft, review and editing. Joan Sander: investigation (quantum chemical studies), writing – original draft, review and editing. Simon Dietzmann: investigation (synthetic and mechanistic studies). Thomas Rittner: investigation (spectroscopic investigations). Jannes Rückel: investigation (synthetic and mechanistic studies). Vanessa R. Landaeta: writing – original draft, review and editing. Jiyong Park: supervision, writing – review and editing. Patrick Nuernberger: supervision, writing – review and editing, funding acquisition. Mu-Hyun Baik: supervision, writing – review and editing. Robert Wolf: conceptualization, writing – review and editing, funding acquisition.

Conflicts of interest

There are no conflicts to declare.

Acknowledgements

We thank Hannes Schneider and David Preitschaft for valuable experimental assistance, Sabrina Dinauer for performing the EPR measurements and the research group of Prof. Burkhard König for technical support. We also acknowledge the support of the Elite Network of Bavaria. This work was funded by the Deutsche Forschungsgemeinschaft (CRC 325 Assembly Controlled Chemical Photocatalysis – 444632635, projects A4 and A5) and the Alexander von Humboldt Stiftung (Georg Förster Research Fellowship, VEN – 1186623 – GF-E). We thank the Institute for Basic Science in Korea for financial support (IBS-R010-A1).

References

- 1 A. Y. Chan, I. B. Perry, N. B. Bissonnette, B. F. Buksh, G. A. Edwards, L. I. Frye, O. L. Garry, M. N. Lavagnino, B. X. Li, Y. Liang, E. Mao, A. Millet, J. V. Oakley, N. L. Reed, H. A. Sakai, C. P. Seath and D. W. C. MacMillan, *Chem. Rev.*, 2022, **122**, 1485.
- 2 C. Förster and K. Heinze, *Chem. Soc. Rev.*, 2020, **49**, 1057.
- 3 O. S. Wenger, *Chem.–Eur. J.*, 2021, **27**, 2270.
- 4 M. Marchi, G. Gentile, C. Rosso, M. Melchionna, P. Fornasiero, G. Filippini and M. Prato, *ChemSusChem*, 2022, **15**, e202201094.
- 5 C. Zhu, H. Yue, J. Jia and M. Rueping, *Angew. Chem., Int. Ed.*, 2021, **60**, 17810.
- 6 K. L. Skubi, T. R. Blum and T. P. Yoon, *Chem. Rev.*, 2016, **116**, 10035.



- 7 H. Luo, Y. Feng and L. Lin, *ChemCatChem*, 2023, **15**, e202300303.
- 8 L. Zou, R. Sun, Y. Tao, X. Wang, X. Zheng and Q. Lu, *Nat. Commun.*, 2024, **15**, 5245.
- 9 A. Y. Chan, A. Ghosh, J. T. Yarranton, J. Twilton, J. Jin, D. M. Arias-Rotondo, H. A. Sakai, J. K. McCusker and D. W. C. MacMillan, *Science*, 2023, **382**, 191.
- 10 B. Ling, S. Yao, S. Ouyang, H. Bai, X. Zhai, C. Zhu, W. Li and J. Xie, *Angew. Chem., Int. Ed.*, 2024, **63**, e202405866.
- 11 H. Wang and T. XU, *Chem Catal.*, 2024, **4**, 100952.
- 12 D. A. Cagan, D. Bim, N. P. Kazmierczak and R. G. Hadt, *ACS Catal.*, 2024, **14**, 9055.
- 13 E. R. Welin, C. Le, D. M. Arias-Rotondo, J. K. McCusker and D. W. C. MacMillan, *Science*, 2017, **355**, 380.
- 14 B. Pieber, J. A. Malik, C. Cavedon, S. Gisbertz, A. Savateev, D. Cruz, T. Heil, G. Zhang and P. H. Seeberger, *Angew. Chem., Int. Ed.*, 2019, **58**, 9575.
- 15 R. Sun, Y. Qin and D. G. Nocera, *Angew. Chem., Int. Ed.*, 2020, **59**, 9527.
- 16 J. Li, C.-Y. Huang and C.-J. Li, *Chem*, 2022, **8**, 2419.
- 17 D. G. Brown and J. Boström, *J. Med. Chem.*, 2016, **59**, 4443.
- 18 A. Parenty, X. Moreau and J.-M. Campagne, *Chem. Rev.*, 2006, **106**, 911.
- 19 W. Cai, B. Chekal, D. Damon, D. LaFrance, K. Leeman, C. Mojica, A. Palm, M. St Pierre, J. Sieser, K. Sutherland, R. Vaidyanathan, J. van Alsten, B. Vanderplas, C. Wager, G. Weisenburger, G. Withbroe and S. Yu, *Transition metal-catalyzed couplings in process chemistry, Case studies from the pharmaceutical industry*, Wiley-VCH, Weinheim, Germany, OP, 2013.
- 20 D. J. C. Constable, P. J. Dunn, J. D. Hayler, G. R. Humphrey, J. J. L. Leazer, R. J. Linderman, K. Lorenz, J. Manley, B. A. Pearlman, A. Wells, A. Zaks and T. Y. Zhang, *Green Chem.*, 2007, **9**, 411.
- 21 L. A. Wolzak, F. J. de Zwart, J.-P. H. Oudsen, S. A. Bartlett, B. de Bruin, J. N. H. Reek, M. Tromp and T. J. Korstanje, *ChemCatChem*, 2022, **14**, e202200547.
- 22 Y. Mo, Z. Lu, G. Rughoobur, P. Patil, N. Gershenfeld, A. I. Akinwande, S. L. Buchwald and K. F. Jensen, *Science*, 2020, **368**, 1352.
- 23 H. Luo, G. Wang, Y. Feng, W. Zheng, L. Kong, Y. Ma, S. Matsunaga and L. Lin, *Chem.-Eur. J.*, 2023, **29**, e202200547.
- 24 X. Zhu, Q. Fan, W. Luo, D. Wang, Y. Jia, H. Li, Z. Wang, Q. Xiao and X. He, *Chin. J. Chem.*, 2023, **41**, 411.
- 25 M. He, S. Yang, X. Yu and M. Bao, *Synlett*, 2022, **33**, 1189.
- 26 W. Zu, C. Day, L. Wei, X. Jia and L. Xu, *Chem. Commun.*, 2020, **56**, 8273.
- 27 J. A. Malik, A. Madani, B. Pieber and P. H. Seeberger, *J. Am. Chem. Soc.*, 2020, **142**, 11042.
- 28 J. Lu, B. Pattengale, Q. Liu, S. Yang, W. Shi, S. Li, J. Huang and J. Zhang, *J. Am. Chem. Soc.*, 2018, **140**, 13719.
- 29 M. A. Bajada, G. Di Liberto, S. Tosoni, V. Ruta, L. Mino, N. Allasia, A. Sivo, G. Pacchioni and G. Vilé, *Nat. Synth.*, 2023, **2**, 1092.
- 30 C. Cavedon, S. Gisbertz, S. Reischauer, S. Vogl, E. Sperlich, J. H. Burke, R. F. Wallick, S. Schrottke, W.-H. Hsu, L. Anghileri, Y. Pfeifer, N. Richter, C. Teutloff, H. Müller-Werkmeister, D. Cambié, P. H. Seeberger, J. Vura-Weis, R. M. van der Veen, A. Thomas and B. Pieber, *Angew. Chem., Int. Ed.*, 2022, **61**, e202211433.
- 31 T.-T. Zhao, H.-N. Qin and P.-F. Xu, *Org. Lett.*, 2023, **25**, 636.
- 32 L. Anghileri, H. Baunis, A. R. Bena, C. Giannoudis, J. H. Burke, S. Reischauer, C. Merschjann, R. F. Wallik, G. Simionato, S. Kovalenko, L. Dell'Amico, R. M. van der Veen and B. Pieber, *ChemRxiv*, 2024, preprint, DOI: [10.26434/chemrxiv-2024-896n0](https://doi.org/10.26434/chemrxiv-2024-896n0).
- 33 H. Na and L. M. Mirica, *Nat. Commun.*, 2022, **13**, 1313.
- 34 I. Ghosh, N. Shlapakov, T. A. Karl, J. Düker, M. Nikitin, J. V. Burykina, V. P. Ananikov and B. König, *Nature*, 2023, **619**, 87.
- 35 N. Sanosa, P. Ruiz-Campos, D. Ambrosi, D. Sampedro and I. Funes-Ardoiz, *Int. J. Mol. Sci.*, 2023, **24**, 9145.
- 36 S. Gisbertz, S. Reischauer and B. Pieber, *Nat. Catal.*, 2020, **3**, 611.
- 37 E. B. Corcoran, M. T. Pirnot, S. Lin, S. D. Dreher, D. A. DiRocco, I. W. Davies, S. L. Buchwald and D. W. C. MacMillan, *Science*, 2016, **353**, 279.
- 38 J. A. Terrett, J. D. Cuthbertson, V. W. Shurtleff and D. W. C. MacMillan, *Nature*, 2015, **524**, 330.
- 39 C. H. Chrisman, M. Kudisch, K. O. Puffer, T. K. Stewart, Y. M. L. Lamb, C.-H. Lim, R. Escobar, P. Thordarson, J. W. Johannes and G. M. Miyake, *J. Am. Chem. Soc.*, 2023, **145**, 12293.
- 40 S. I. Ting, W. L. Williams and A. G. Doyle, *J. Am. Chem. Soc.*, 2022, **144**, 5575.
- 41 Y. Qin, R. Sun, N. P. Gianoulis and D. G. Nocera, *J. Am. Chem. Soc.*, 2021, **143**, 2005.
- 42 N. A. Till, S. Oh, D. W. C. MacMillan and M. J. Bird, *J. Am. Chem. Soc.*, 2021, **143**, 9332.
- 43 N. A. Till, L. Tian, Z. Dong, G. D. Scholes and D. W. C. MacMillan, *J. Am. Chem. Soc.*, 2020, **142**, 15830.
- 44 R. Sun, Y. Qin, S. Ruccolo, C. Schnedermann, C. Costentin and D. G. Nocera, *J. Am. Chem. Soc.*, 2019, **141**, 89.
- 45 D. A. Cagan, D. Bim, B. J. McNicholas, N. P. Kazmierczak, P. H. Oyala and R. G. Hadt, *Inorg. Chem.*, 2023, **62**, 9538.
- 46 D. A. Cagan, D. Bim, B. Silva, N. P. Kazmierczak, B. J. McNicholas and R. G. Hadt, *J. Am. Chem. Soc.*, 2022, **144**, 6516.
- 47 S. I. Ting, S. Garakyaraghi, C. M. Taliaferro, B. J. Shields, G. D. Scholes, F. N. Castellano and A. G. Doyle, *J. Am. Chem. Soc.*, 2020, **142**, 5800.
- 48 L. Yang, H.-H. Lu, C.-H. Lai, G. Li, W. Zhang, R. Cao, F. Liu, C. Wang, J. Xiao and D. Xue, *Angew. Chem., Int. Ed.*, 2020, **59**, 12714.
- 49 R. D. Bradley, B. D. McManus, J. G. Yam, V. Carta and A. Bahamonde, *Angew. Chem.*, 2023, **135**, e202310753.
- 50 M. Grübel, I. Bosque, P. J. Altmann, T. Bach and C. R. Hess, *Chem. Sci.*, 2018, **9**, 3313.
- 51 R. Lauenstein, S. L. Mader, H. Derondeau, O. Z. Esezobor, M. Block, A. J. Römer, C. Jandl, E. Riedle, V. R. I. Kaila, J. Hauer, E. Thyrhaug and C. R. Hess, *Chem. Sci.*, 2021, **12**, 7521.



- 52 D. Zhao, W. Wang, F. Yang, J. Lan, L. Yang, G. Gao and J. You, *Angew. Chem., Int. Ed.*, 2009, **48**, 3296.
- 53 D. Zhao, W. Wang, S. Lian, F. Yang, J. Lan and J. You, *Chem. – Eur. J.*, 2009, **15**, 1337.
- 54 M. Mokfi, J. Rust, C. W. Lehmann and F. Mohr, *Molecules*, 2021, **26**, 3705.
- 55 R. A. Altman, E. D. Koval and S. L. Buchwald, *J. Org. Chem.*, 2007, **72**, 6190.
- 56 D. Xue, Z.-H. Jia, C.-J. Zhao, Y.-Y. Zhang, C. Wang and J. Xiao, *Chem. – Eur. J.*, 2014, **20**, 2960.
- 57 A. Böhm and T. Bach, *Chem. – Eur. J.*, 2016, **22**, 15921.
- 58 E. L. B. Johnson Humphrey, A. R. Kennedy, S. Sproules and D. J. Nelson, *Eur. J. Inorg. Chem.*, 2022, **2022**, e202101006.
- 59 Q. Lin and T. Diao, *J. Am. Chem. Soc.*, 2019, **141**, 17937.
- 60 M. Mohadjer Beromi, G. W. Brudvig, N. Hazari, H. M. C. Lant and B. Q. Mercado, *Angew. Chem., Int. Ed.*, 2019, **58**, 6094.
- 61 A. Bismuto, P. Müller, P. Finkelstein, N. Trapp, G. Jeschke and B. Morandi, *J. Am. Chem. Soc.*, 2021, **143**, 10642.

